IEEE Open Journal of Antennas and Propagation

Received XX Month XXXX; revised X Month XXXX; accepted XX Month XXXX. Date of publication XX Month XXXX; date of current version XX Month XXXX.

*Digital Object Identifier 10.1109/OAJPE.2020.2976889*

# Reconfigurable Antenna Booster System for Multiband Operation in IoT Devices with an SP4T Switch

**ELENA GARCIA[1], AURORA ANDÚJAR[1], JOAN L. PIJOAN[2], JAUME ANGUERA[1,2], IEEE FELLOW**

[1] Ignion, Barcelona, Spain

[2] Smart Society Research Group, Universitat Ramon Llull, Barcelona, Spain

Elena García is with Ignion, 08190 Barcelona, Spain (elena.garcia@ignion.io). Aurora Andújar is with Ignion, 08190 Barcelona, Spain (aurora.andujar@ignion.io). Jaume Anguera (corresponding author) is with Ignion, 08190 Barcelona, Spain (jaume.anguera@ignion.io) and La Salle Engineering – Universitat Ramon Llull, 08022 Barcelona, Spain. Joan L- Pijoan is with La Salle Engineering – Universitat Ramon Llull, 08022 Barcelona, Spain (joanlluis.pijoan@salle.url.edu).

This work was supported by the Industrial Doctorate Plan of the Secretariat of Universities and Research of the Department of Business and Knowledge of the Generalitat of Catalonia (Reference 2021 DI 23). Mentions to Qorvo for the S-parameters data of the switch and the QM13345 samples.

**ABSTRACT** The increase in the IoT (Internet of Things), such as trackers and sensors, puts pressure on device dimensions and performance. This is translated to the antenna system since it has to be both efficient and provide operation across different frequency bands. However, these antennas must also be small enough to fit into the limited space available in wireless devices. To address this challenge, a reconfigurable architecture with a single SP4T (Single-Pole 4-Throw) operating at 698 MHz – 960 MHz and 1710 MHz – 2170 MHz is proposed, designed, and built embedding a 30 mm x 3 mm x 1 mm (0.07λ) non-resonant element called an antenna booster element. This approach does not require antennas with complex geometric shapes to achieve multiband behavior. Instead, they rely on a multiband matching network to achieve efficient operation across multiple frequency bands. This design approach is easier, faster, and simpler than creating a new antenna for every device. Additionally, the reconfigurable matching network allows an easy configuration and optimization of frequency bands. The analysis shows the advantages of the reconfigurable solution compared to a non-reconfigurable one for a 75 mm x 60 mm printed circuit board (PCB).

**INDEX TERMS** Small, multiband, and reconfigurable antennas, matching networks, and antenna boosters.

## I. INTRODUCTION

Using complex geometries to design small and multiband antennas is one of the most common methods. The frequency bands of operation depend on the resonant modes of such antenna [1]-[8]. To simplify the design, antenna boosters were proposed [9]-[14], where the frequency bands of operation are controlled by the design of a matching network, which is easier and faster than designing an antenna based on complex geometries. Essentially, an antenna booster features a non-resonant impedance, typically at the lowest frequency bands. The frequency bands of operation can then be tuned by designing a proper matching network.

In specific scenarios where a small ground plane is necessary (~0.1λ in length at the lowest frequency of operation), employing an antenna booster and a passive matching network might not be sufficient to satisfy the required bandwidth. Hence, a reconfigurable antenna booster solution is proposed to solve this issue. This proposal is convenient for IoT devices where the size of the device is small or the number of frequency bands is large, which makes this situation difficult for a passive antenna system.

Various methodologies have been employed in the design of reconfigurable antenna systems [15]-[38], Among these, PIN diodes are the most prevalent, utilized in 58% of cases, followed by digital tunable capacitors (DTC) at 25%, and RF MEMS switches at 29%. PIN diodes, due to their ON and OFF states, are more suitable for providing multiband operation rather than a smooth, tunable solution, as is the case with MEMS switches and DTC due to the larger number of states.

In [17], a 25x25 mm$^2$ resonant antenna is reported. The reconfigurable design is achieved by three PIN diodes using four states, and the combinations of these diodes enable operation at 3.82 GHz, 4.11 GHz, 4.48 GHz, 4.90 GHz, and 6.04 GHz. The antenna presents a size of 0.3λ at the lowest frequency of operation.

The work proposed in [18] is a 35x25 mm$^2$ antenna with two PIN diodes, using three states, and the frequency bands are 1.98 – 2.51 GHz, 2.52 – 6.02 GHz, 3.97 – 7.87 GHz, and 7.1 – 10.7 GHz. In this case, the antenna is 0.23λ at the lowest frequency of operation.

In [19], a reconfigurable antenna with a size of 135x83 mm$^2$ and two PIN diodes, four states, is proposed operating

in 1.57 – 2.15 GHz, 2.13 – 3.0 GHz, 3.17–3.43 GHz, 5.2 – 5.8 GHz, 6.3 – 6.78 GHz, 8.31 – 8.90 GHz, 9.04 – 9.58 GHz, and 12.03–13.14 GHz bands. In this case, the antenna is 0.7λ at the lowest frequency of operation.

The antenna proposed in [20] features 37.5x21 $mm^2$ and uses one PIN diode and two states; the operating bands are 1.2 – 1.4 GHz, 1.6 – 1.9 GHz, 2.3 – 2.8 GHz, 2.6 – 3.6 GHz, and 4.5 – 5 GHz. In this case, the antenna is 0.15λ at the lowest frequency of operation.

In [21], a reconfigurable resonant antenna 30x60 $mm^2$ size, 0.36λ, with four PIN diodes, using five states, the operating frequencies are 1.8 GHz, 2.4 GHz, 3.5 GHz, and 5.2 GHz, is analyzed. In [22], two designs based on antenna boosters are proposed. First, a solution using digitally tunable capacitors and eight lumped components (capacitors and inductors), with four states in use, covering 698 – 960 MHz and 1710 – 2690 MHz in a 131x60 $mm^2$ PCB. Secondly, a solution with two SP8T switches and nine lumped components, six states in use, covering 698 – 960 MHz, 1710 – 2170 MHz, and GPS 1575 MHz, in a 50x50 $mm^2$ PCB and a 12x40 $mm^2$ clearance area. In [23], a reconfigurable antenna is obtained by introducing two parasitic inverted-L grounded strips and a PIN diode, two states, into a 130x67 $mm^2$ PCB. The clearance area is 14x67 $mm^2$, and the frequency range is 824 – 960 MHz and 1710 – 2690 MHz.

In [24], a U-shape slot of 1mm wide is designed in a PCB of 143x74 $mm^2$ without clearance area and connected to an SP4T switch, four states, that is grounded. It uses eight lumped components, and the frequency ranges are 690 – 960 MHz and 1700 – 2700 MHz.

Other single-band tunable solutions with DTC are investigated [25], [26], and there is a comparison between the ones with the same operational bands in the discussion section V. As observed from the prior art, either the antenna size and PCB is large, or the number of switches and lumped components is significant. As shown in all previous cases, antenna size is comparable to the wavelength.

To further increase the simplicity of the solution, a new architecture featuring a compact 30 x 3 x 1 $mm^3$, 0.07λ antenna booster element, an SP4T, and only five lumped components on a small 75 mm x 60 mm PCB is presented. Such architecture can provide operation at 698 MHz – 960 MHz and 1710 MHz – 2170 MHz, which is widely used for IoT applications [39].

The paper, which is a detailed extension of the conference paper in [40], is structured as follows: about the non-resonant impedance on the antenna booster element is presented in section II; the proposed design of the reconfigurable antenna architecture using one SP4T from the simulation domain is described in section III; the hardware implementation is explained in section IV; the discussion comparing a passive solution with the new reconfigurable solution is in section V; finally, conclusions are drawn in section VI.

## II. ABOUT THE ANTENNA BOOSTER ELEMENT

In contrast to conventional antenna design, which typically involves creating a λ/4 monopole to resonate at the desired frequency, the booster antenna element employs a distinctive approach. This element, fashioned as an FR4 fixed component measuring λ/14, incorporates a designed matching network featuring lumped components like inductors and capacitors. This network can be tuned to cover from 400 MHz to 8000 MHz, depending on the specific tuning parameters.

Reference [41] illustrates the distinctions between a complex geometry antenna and an antenna booster. The complex geometry antenna, being resonant, exhibits multiple resonances. Consequently, in regions where resonance is not achieved, there is a significant loss of efficiency. In contrast, antenna boosters are non-resonant, allowing for matching to the frequency of interest by modifying the matching network. This adaptability ensures that no losses are incurred. A more detailed comparison is included in [41].

In this case, a 30 mm x 3 mm x 1 mm (height) non-resonant antenna booster element is used (Figure 1) for achieving multiband performance from 698 MHz – 960 MHz up to 1710 MHz – 2170 MHz. This element comprises two ports, the RF port and Port 1, introducing a level of flexibility into the design. It allows for the incorporation of an additional component (e.g., inductor, capacitor, open or short) at Port 1, as explained next.

The recommended operation is as follows: for single-band operation below 1GHz, port 1 is short-circuited, and a matching network is added in the RF port. For multi-band operation, as in the present case, port 1 includes an LC filter. Details on how to optimize the filter at port 1 are detailed next.

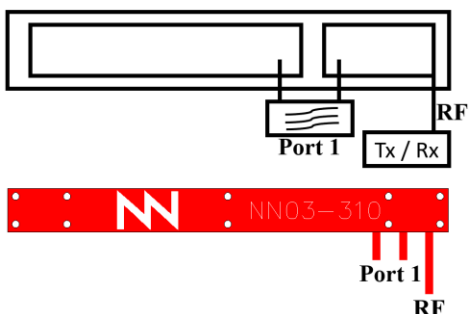


**FIGURE 1. A 30 mm x 3 mm x 1 mm antenna booster element [13].**

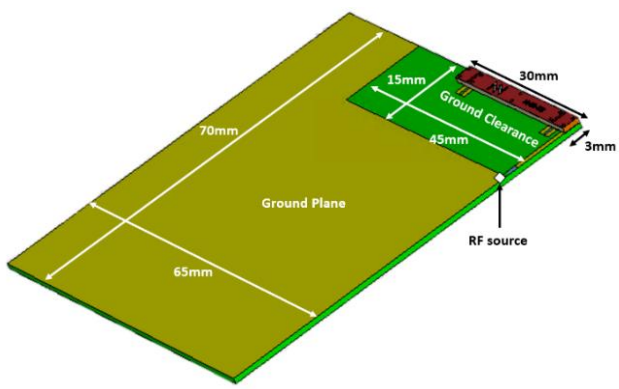


**FIGURE 2. A 30 mm x 3 mm x 1 mm (height) antenna booster element. The 70mm x 65mm x 1mm PCB comprises an FR4 substrate 1 mm thick ($\varepsilon_r$=4.15, tanδ=0.02) with a 15mm x 45mm clearance area.**

The antenna booster element is integrated into a 70 mm x 65 mm PCB and a 15 mm x 45 mm ground clearance (Figure 2). Said antenna booster element is in charge of exciting radiating modes in the ground plane, which becomes the relevant part of the radiation process [9]-[14].

When port 1 is shorted with 0Ω, the impedance at the low-frequency region (698 MHz – 960 MHz) is in the capacitive region. Conversely, the impedance at the high-frequency region is high (~200Ω) due to a second-order mode (Figure 3).

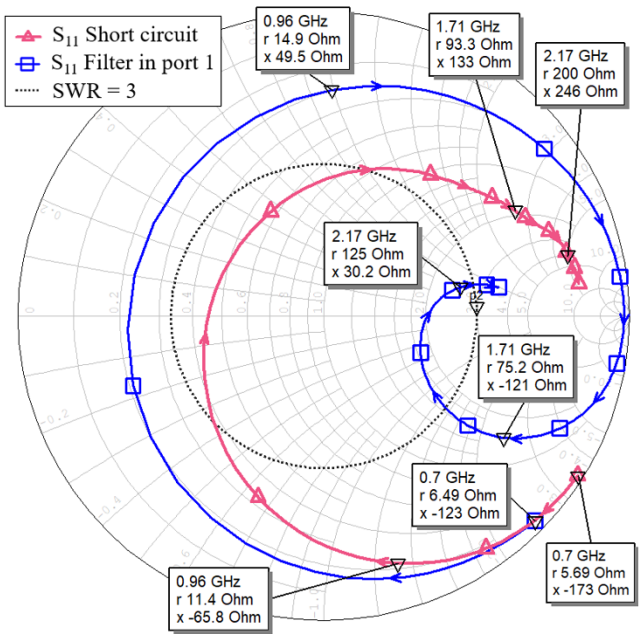


**FIGURE 3. Input impedance of the antenna booster shown in Figure 1 with, in dashed pink, short-circuited at ports 1, and in blue, port 1 with filter L=15nH, C=0.3pF ($f_{notch}$=2.37GHz).**

However, this behavior can be changed with an LC filter at port 1 to make the high-frequency region impedance locus closer to the center of the Smith chart.

In practical terms, incorporating an LC filter with a notch at the second frequency region (~2.37GHz) transforms the impedance into a configuration resembling that of a first-order mode, as confirmed by the potential bandwidth calculations. It is noteworthy that achieving an impedance nearly inside an SWR<3 ($S_{11}$<-6dB) circle at the Smith chart simplifies the overall impedance matching (Figure 3). In the context of IoT devices, SWR<3 ($S_{11}$<-6dB) is considered a reference for bandwidth computations. Failing to achieve an SWR of less than 3 results in a notable decrease in transmitted power. At SWR=3, the delivered power to the antenna system is 75%, with the remaining 25% reflected. Contrastingly, at SWR=4, the delivered power diminishes to 64%, which is 0.7dB less.

$$Q_a(\omega) = \frac{\omega}{2R(\omega)} \sqrt{\left[\frac{dR(\omega)}{d\omega}\right]^2 + \left[\frac{dX(\omega)}{d\omega} + \left|\frac{X(\omega)}{\omega}\right|\right]^2} \quad (1)$$

$$BW = \frac{f_2 - f_1}{f_o} = \frac{SWR - 1}{Q_a\sqrt{SWR}} \quad (2)$$

The bandwidth potential can estimate the obtainable bandwidth given the input impedance of the antenna system [38]. There are different methods to calculate this bandwidth potential; one is with the (1) and (2), where R(ω) and X(ω) are the simulated input impedances of the antenna. Another viable approach is to design an impedance matching in the antenna system at a given frequency using one or two lumped components. This process can be obtained with Optenni-Lab. It's worth noting that both methods yield comparable results (Figure 4), notably below 2.2 GHz, both methods exhibit a strong agreement. However, in the frequency region between 2.2 GHz and 2.7 GHz, the BW potential obtained with Eq. (1)-(2) diverges.

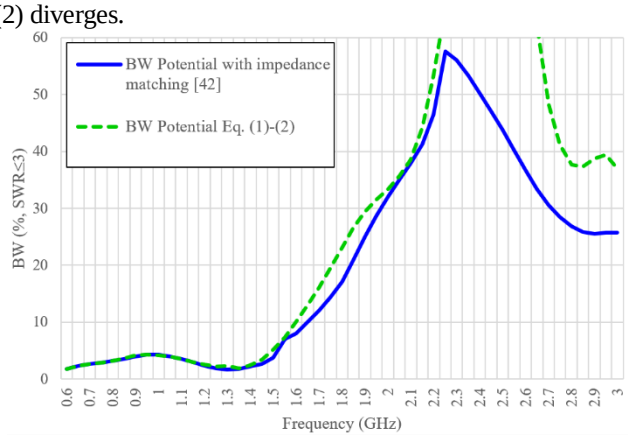


**FIGURE 4. Obtained bandwidth for a PCB of 70x65 mm² with a clearance area of 15x45 mm² with antenna booster shown in Fig. 1. With a filter in port 1 of 0.3pF and 15nH.**

This is due to impedance loops that make derivatives in Eq. (1) diverge, as explained in [42]. Nevertheless, despite these occasional discrepancies, Eq. (1) is also simple, fast, and helps understand how much bandwidth can be obtained. Furthermore, in regions where the results diverge, it indicates that a significant bandwidth can be obtained. Consequently, in such cases, exploring more precise methods, like those involving impedance matching with one or two lumped components, becomes imperative to ascertain the actual bandwidth potential.

In (Figure 5), the effects of the filter in port 1 of the antenna booster element are discussed. When no filter is present, there is no impact in the low-frequency region. However, even though the requirement of 23.7% bandwidth is achieved in the high-frequency region, the bandwidth is higher with a filter.
In (Figure 5 a), it's important to note that only the inductor is altered while keeping the capacitor constant, so the central frequency differs in each case. Given the need for a 23.7% bandwidth in the high-frequency region, the filter with the central frequency at 2.65GHz does not pass this target. On the other hand, the filter with the central frequency at 2.16 GHz decreases the bandwidth at 900MHz.

In (Figure 5 b), all three filters share a common central frequency of 2.37GHz. When the inductor is reduced to 11nH and the capacitor is increased to 0.4pF, it fails to achieve the desired 23.7% bandwidth. Conversely, in the case of a higher inductor value of 22nH and a lower capacitor value of 0.2pF,

the bandwidth decreases at 900 MHz. In both scenarios, the filter of 0.3pF and 15nH does not decrease the bandwidth at the low-frequency region and passes the 23.7% bandwidth at the high band, with a central frequency of 2.37GHz. Thus, this filter configuration is selected as the most suitable option. Furthermore, even though the average bandwidth potential remains similar to the case without a filter, the introduction of the filter results in the input impedance aligning closer to the center of the Smith chart (Figure 3). As a result, the filter is the preferred option.

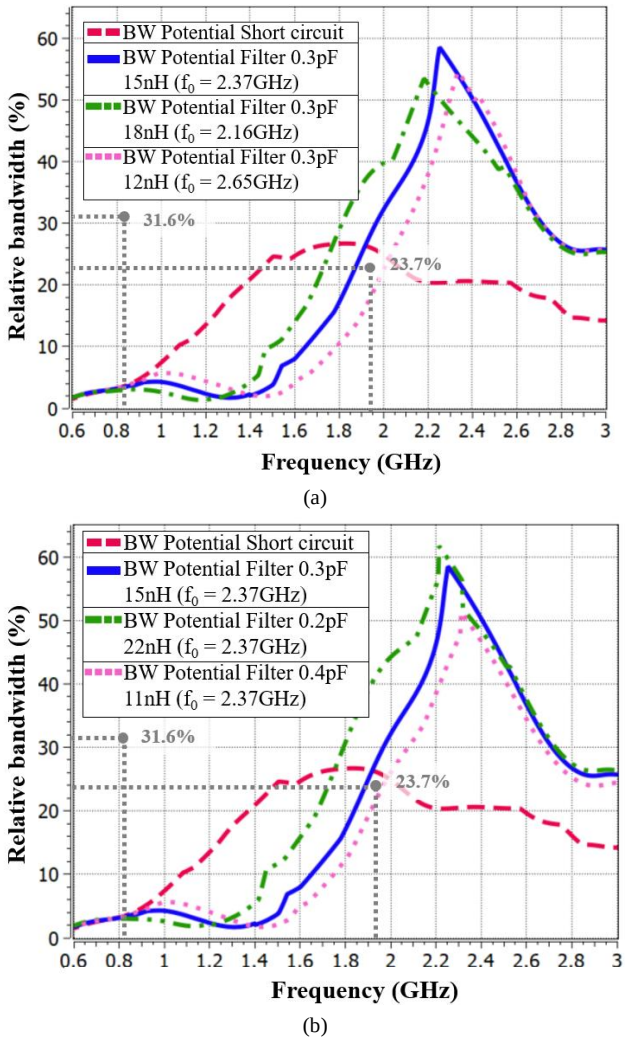


**FIGURE 5. Relative bandwidth potential obtained by Optenni Lab [42] at SWR=3 of the PCB with antenna booster shown in Fig. 1. The red dashed line is with port 1 short-circuited, and the others are with port 1 with a filter. $f_0$ corresponds to the notch filter. a) filters with different resonant frequencies; b) with the filter with $f_0$=2.37 GHz but with different LC pairs.**

In conclusion, with a passive matching network, it is not possible to have an SWR<3 across the entire low and high-frequency regions, so it is not feasible to match since the potential bandwidth is 5%, whereas the requested bandwidth is 31.6%. Thus, a reconfigurable architecture is proposed to achieve performance in the low-frequency region 698 MHz – 960 MHz, needing seven different matching networks to operate correctly (Table I). Hence, the introduction of a reconfigurable architecture becomes imperative.

TABLE I
BANDWIDTH POTENTIAL DIVIDED INTO 7 STATES

| $f_{Min\ (MHz)}$ | $f_{Max\ (MHz)}$ | $f_{Central\ (MHz)}$ | $BW_{potential}$ |
|---|---|---|---|
| 698 | 733 | 715.5 | 5% |
| 733 | 770 | 751.5 | 5% |
| 770 | 809 | 789.5 | 5% |
| 809 | 850 | 829.5 | 5% |
| 850 | 893 | 871.5 | 5% |
| 893 | 938 | 915.5 | 5% |
| 938 | 962 | 950 | 3% |

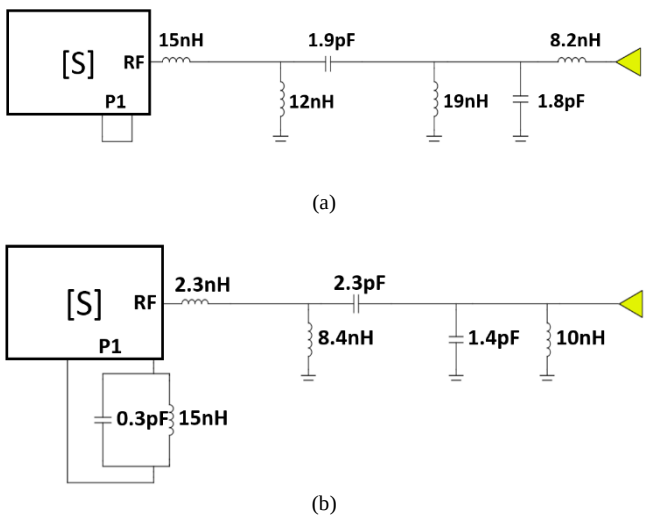


**FIGURE 6. Matching networks to match 698 MHz – 960 MHz and 1710 MHz – 2170 MHz for the antenna system shown in Fig. 1. [S] represents the impedance of the antenna system in Fig. 2 without any matching network. "a" is with port 1 short-circuited, and "b" is with the filter obtained before in port 1.**

TABLE II
WORST QUALITY FACTOR Q IN THE FREQUENCY RANGE OF INTEREST (698 – 2170 MHZ) OF THE COMPONENTS IN FIG. 6.

| *19nH* | *15nH* | *12nH* | *10nH* | *8.4nH* | *8.2nH* | *2.3nH* |
|---|---|---|---|---|---|---|
| 75 | 79 | 80 | 84 | 85 | 72 | 66 |
| **2.3pF** | | **1.9pF** | **1.8pF** | | **1.4pF** | **0.3pF** |
| 173 | | 168 | 179 | | 221 | 570 |

To compare the benefit of the filter at port 1 of the antenna booster element (Figure 1), a passive matching network to match from 698 MHz to 960 MHz and from 1710 MHz to 2170 MHz is designed with a matching network synthesizer [42] (Figure 6). The synthesis process considers real SMD (Surface Mounted Devices) inductors and capacitors from Murata. SMDs are used because they are small components (1mm x 0.5 mm) with a high-quality factor (Q). In Table II, the worst Q for each component used in (Figure 6) can be

observed. It is noticeable that the inductors exhibit significantly lower Q values compared to the capacitors.

In Figure 6a, the best matching network is displayed, considering port 1 short-circuited, while Figure 6b considers the previously studied filter with values of 0.3pF and 15nH at port 1.

The $S_{11}$ simulations illustrate that the passive matching network falls short of achieving adequate matching, particularly in covering the low-frequency region (Figure 7). A noticeable disparity is observed when comparing the performance with Port 1 short-circuited to that with the filter in place, the filter allows covering all the high-frequency bands with a good $S_{11}$. Moreover, it improves the low-frequency band. However, it remains insufficient to provide complete coverage in the low-frequency region.

Consequently, a reconfigurable solution is essential to address the challenge of covering the low-frequency band (698 MHz – 960 MHz). Despite the initial prediction of a 5% bandwidth potential at 800 MHz, the necessity to also match the high-frequency region results in inadequate matching in the low band, failing to reach the desired -6dB. This reaffirms the necessity for a reconfigurable architecture, addressed in the next section.

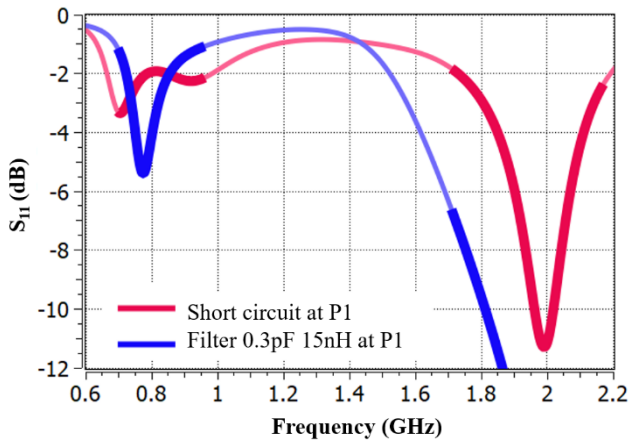


**FIGURE 7. Simulated reflection coefficient of the antenna booster system shown in Fig. 1 with the passive matching network shown in Fig. 4.**

## III. RECONFIGURABLE ARCHITECTURE

A reconfigurable system embedding the antenna booster element explained before is designed with a 70mm x 65mm PCB, an SP4T switch, and a matching network to obtain an $S_{11}$<-6dB across 698 MHz – 960 MHz and 1710 MHz – 2170 MHz. Although the $S_{11}$ is a good figure of merit, it is not enough to validate the electromagnetic performance of the wireless device. In this regard, total efficiency ($\eta_t$), which takes into account $S_{11}$ and radiation efficiency ($\eta_r$), is used: $\eta_t=\eta_r\cdot(1-|S_{11}|^2)$. The question is if there is a minimum level of efficiency that can be used as a target.

In the realm of IoT devices, many devices must be certified in terms of TRP/TIS [43]. The TRP (Total Radiated Power) required for NB-IoT in free space for small form-factor devices under 107mm in the longest direction are in the low band 698 MHz – 960 MHz, 10dBm, and in the high-frequency band 1710 MHz – 2170 MHz, 12dBm. That means that with an estimated RF module output power of 23dBm, the total efficiency needed is 5% in the low-frequency band and 8% in the high-frequency band.

The objective is to attain a total efficiency exceeding 5% and 8%, respectively, to account for potential losses introduced by additional plastic materials in the final device. It is important to note that the measured [S] parameters of the SP4T are included in the electromagnetic simulation (FIGURE 8).

The design consists of four lumped components (capacitors and inductors) between the antenna booster element and the SP4T switch and a shunt inductor on the common input/output of the SP4T [15].

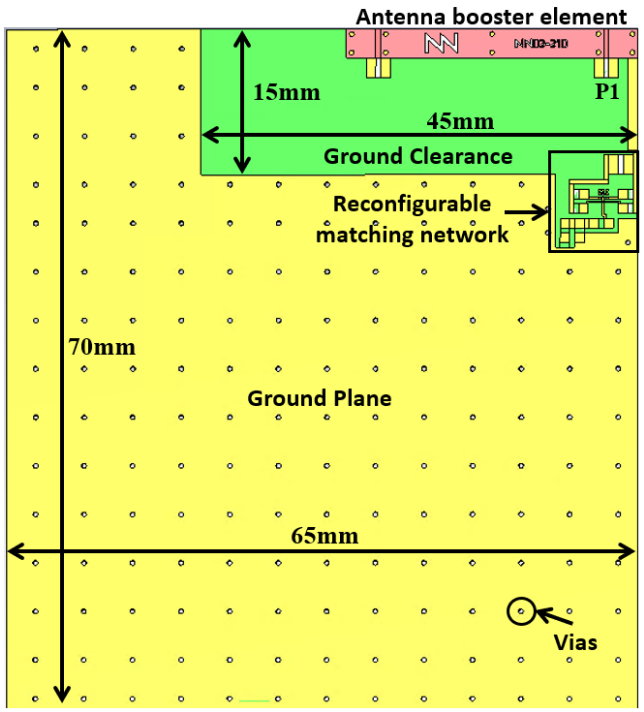


**FIGURE 8. 70 mm x 65mm x 1mm PCB (top layer), with a 15 mm x 45 mm clearance area. The antenna booster element is situated on the top right, and the SP4T switch QM13345 is situated after the antenna feeding line. The yellow represents the ground plane, the green represents the ground clearance area, and the red represents the antenna booster chip component. The substrate (in green color and extending between the top and bottom layer) is 1mm thick, $\varepsilon_r$=4.15, and tanδ=0.02.**

The electromagnetic simulation considers the entire layout, including the transmission lines for the matching network, pads for allocating the switch, and vias to the bottom, later hosting the common matching network. The antenna booster element, the switch, and the four lumped components connected to RF1, RF2, RF3, and RF4 of the switch are located on the top layer. The common matching network connected to the common input/output port of the switch is placed on the bottom layer. Both ground layers of the top and bottom layers are connected through 0.25mm diameter vias

and separated from one another by 5mm (~λ/27 at the highest frequency of operation, 2.17 GHz).

To maximize the total efficiency, all components are high-Q, considering multilayer ceramic capacitors and the inductors with a minimum Q of 60 within the frequency band of operation. The components' sizes are 0402 (1 mm x 0.5 mm) and 0603 (1.6 mm x 0.8 mm), making them well-suited for placement on small PCBs such as those found in IoT devices (Figure 8).

The RF switch in use, QM13345, is an SP4T and has a Mobile Industry Processor Interface (MIPI), the insertion loss is 0.13dB in 780 MHz and 0.22dB in 1940 MHz. Internally, this SP4T incorporates 8 switches, enabling a total of $2^8$ possible combinations, so 256 states. Specifically, it utilizes 4 switches in series and 4 others grounded, as shown in (Figure 9). Notably, not all these states are usable in practice. Certain conditions must be met to ensure proper functionality, for instance, it's imperative to have at least one serial switch (SW1S, SW2S, SW3S, SW4S) connected, as leaving all serial switches open would result in an open circuit in RFC. An example of an incorrect connection would be having SW1S, SW2S, SW3S, and SW4S all in the OFF position while having SW1P and SW3P in the ON position. Moreover, it is not practical to have the same serial and ground switch number connected at the same time because this would effectively short-circuit the RFC.

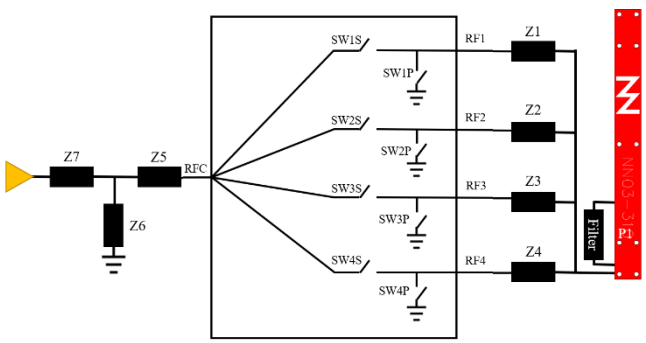


**FIGURE 9. RF SP4T Switch design with all matching networks.**

TABLE III
VALUES OF THE MATCHING NETWORK IN FIG. 8

| *Z1* | *Z2* | *Z3* | *Z4* | *Z5* | *Z6* | *Z7* |
|---|---|---|---|---|---|---|
| 2.1pF | 6pF | 0Ω | 3.7nH | 0Ω | 3.7nH | 0Ω |

For instance, having SW1S, SW2S, SW3S, and SW4S all in the OFF position while having SW1P and SW3P in the ON position or having SW1S and SW4S ON while having SW1P and SW3P ON would be incorrect. However, some valid combinations can be related to (Figure 9), including:

- SW2S, SW3S, SW1P ON and the rest OFF, as a result, Z1 would be shunted and Z2 and Z3 would be in parallel.
- SW1S ON and the rest OFF, as a result, Z1 would be in series.
- SW4S, SW2P, SW3P ON and the rest OFF, as a result, Z2 and Z3 would be shunted and Z4 would be in serial.

It turns out that the number of combinations with the SP4T is 65, which means 65 different matching networks (15 considering series components and 50 considering shunt and series components).

The layout design incorporates four electrically short transmission lines, which notably impact all matching networks. Such transmission lines are needed to connect the feeding line to each of the four ports of the switch (Figure 10). Since those transmission lines are electrically short, they behave as inductances L1, L2, L3, and L4.

It is important to note that the matching networks used on the PCB for measurement remain consistent with those originally derived from the electromagnetic simulation design (CST). The employed matching networks are displayed in (Figure 11). The values of Z1, Z2, Z3, Z4, Z5, Z6, and Z7 are found considering the impedance in each RF output and tunning each matching network. First, the impedance at 698 MHz – 730 MHz is moved from the capacitive zone of the Smith chart to inside the SWR<3 circle (Figure 3) by adding a series (Z4) and shunt (Z6) inductor (Figure 11 a).

Second, the 900 MHz – 960 MHz impedance is moved from the inductive zone of the Smith chart to inside the SWR<3 circle (Figure 3) by adding a series (Z1) capacitor and the common Z6 inductor (Figure 11 f).

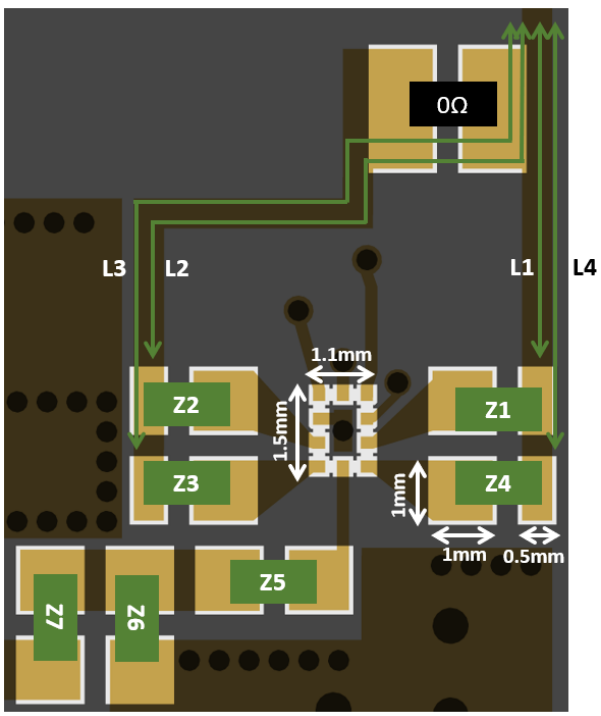


**FIGURE 10. SP4T layout design showing the transmission lines. Zi represents a lumped component (Table III): Z1-Z4 are the components connected between the SP4T and the antenna booster element, and the series Z5, shunt Z6, and series Z7 are the components for the common matching network for fine-tuning purposes. The final proto uses Z5=Z7=0Ω and only Z6 is used with 3.7nH.**

Next, the high-frequency region (1710 MHz – 2170 MHz) is matched using a higher series capacitance than the Z1

capacitor, as the impedance is closer to the SWR<3 circle than previously, and the same Z6 shunt inductor, Z2, is found (Figure 10 g).

Finally, the rest of the lower-frequency region is matched by combining Z1, Z2, and Z4 components (Figure 11 b, c, d & e). The specific design values are outlined in Table III, and the different matching networks are presented in (Figure 11).

To illustrate the switching, an example of one of the seven different matching networks is presented in (Figure 12), representing the matching network from Figure 11 d.

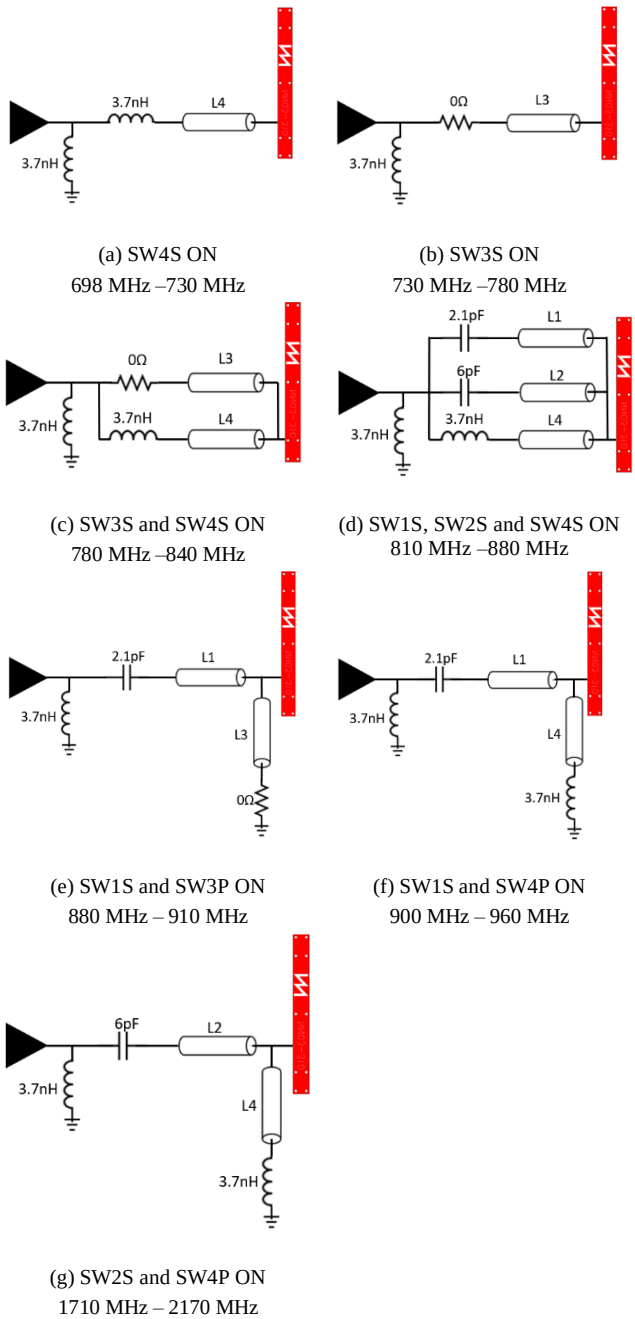


**FIGURE 11. The seven matching networks created by changing the SP4T states, each one adapts a different frequency range. Note that the transmission lines L1-L4 correspond to those given in Fig. 10.**

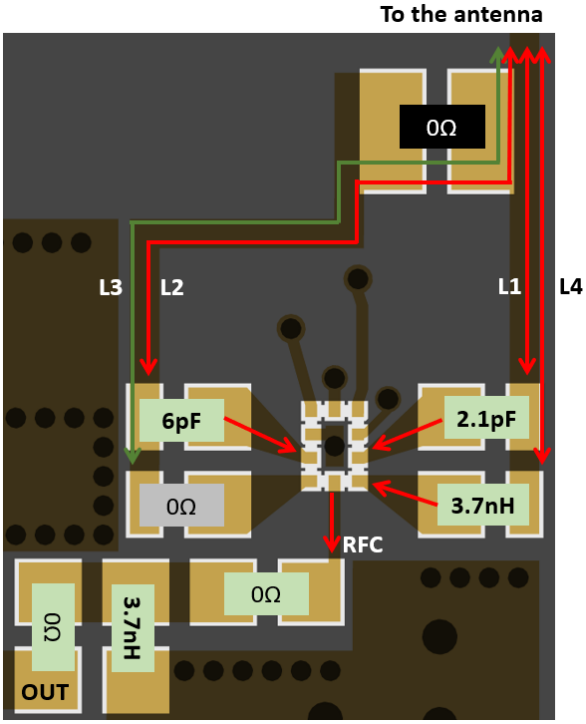


**FIGURE 12. Example of the matching network in Fig. 11 (d).**

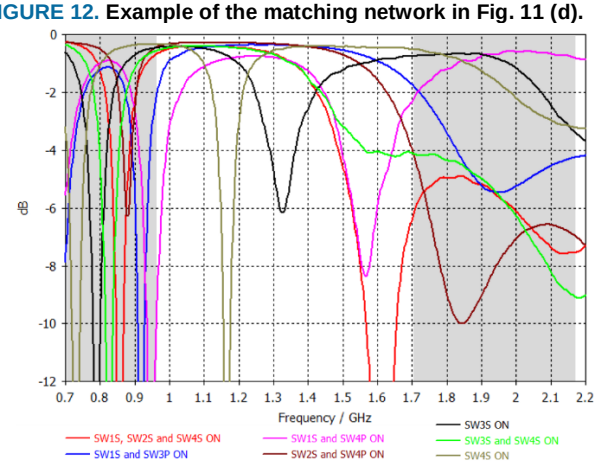


**FIGURE 13. The simulated $S_{11}$ for the seven used states of the SP4T.**

As a result of this design, the simulated $S_{11}$ achieves a -6dB at the frequency regions of interest 698 MHz – 960 MHz and 1710 MHz – 2170 MHz (Figure 13). This solution requires only six states to cover all frequency bands, aligning well with the predictions outlined in Section II, Table-I. For other IoT applications with different frequency bands, the design process will require the same steps explained to achieve the desired matching performance.

## IV. HARDWARE IMPLEMENTATION

The implemented PCB has the same characteristics as the simulated, 70 mm x 65 mm, with a 15 mm x 45 mm clearance area (Figure 14). To ensure a stable voltage supply to the switch, a DCDC converter is connected to a standard 3V

battery, providing the necessary 1.8V required for the SP4T switch.

This solution includes an SP4T from Qorvo (QM13345) with a MIPI interface. The SP4T is controlled by an interface connected to a laptop. Once a particular state is set, the interface is removed so as not to interfere with the $S_{11}$ and efficiency measurements. To keep the SP4T activated, a built-in battery is embedded in the PCB (Figure 14 b).

As a result of these measurements, an S11<-6dB has been achieved at the frequency regions of interest 698 MHz – 960 MHz and 1710 MHz – 2170 MHz (Figure 15), considering the components used in the simulation scenario.

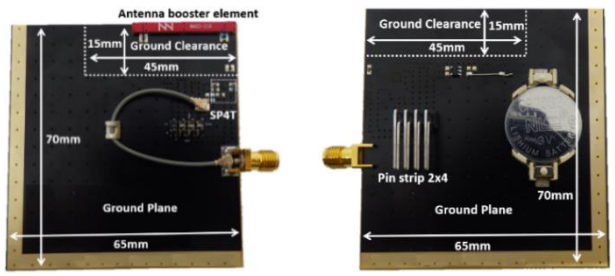


(a) (b)

**FIGURE 14. Prototype of the 70mm x 65mm x 1mm FR4 ($\varepsilon_r$=4.15, and tanδ=0.02) PCB, with a 15mm x 45mm clearance area. "a" is the top layer, and "b" is the bottom layer.**

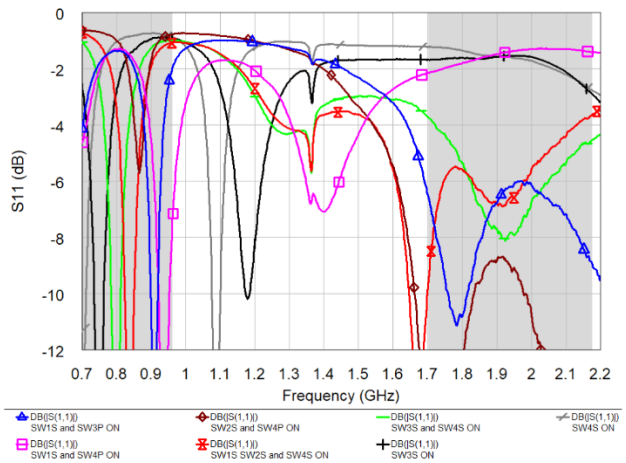


**FIGURE 15. Measured $S_{11}$ of the states in use of the RF switch in the PCB prototype.**

TABLE IV
DEVIATION BETWEEN SIMULATED AND MEASURED $S_{11}$ PARAMETERS

| *State* | *Simulated* $f_{Central\ (MHz)}$ | *Measured* $f_{Central\ (MHz)}$ | *Deviation* |
|---|---|---|---|
| SW4S ON | 726 | 722 | 3% |
| SW3S ON | 788.5 | 775 | 4% |
| SW3S and SW4S ON | 825 | 824 | 2% |
| SW1S, SW2S and SW4S ON | 857 | 862 | 1% |
| SW1S and SW3P ON | 917.5 | 928 | 1% |
| SW1S and SW4P ON | 949 | 967 | 1% |

In particular, this solution only requires seven states to cover all the frequency bands, aligning with the predictions presented in Section II-Table I. When comparing the simulated $S_{11}$ (Figure 13) with the measured $S_{11}$ (Figure 15), Table IV is generated, highlighting the deviation of each state. It is evident from this comparison that the maximum deviation is 4%, which falls well within an acceptable range.

A tolerance analysis is carried for the SW3S ON state (Figure 16) involving 2000 circuit evaluations, considering the components tolerance, typically 2% with normal distribution. This result highlights the robustness of this solution.

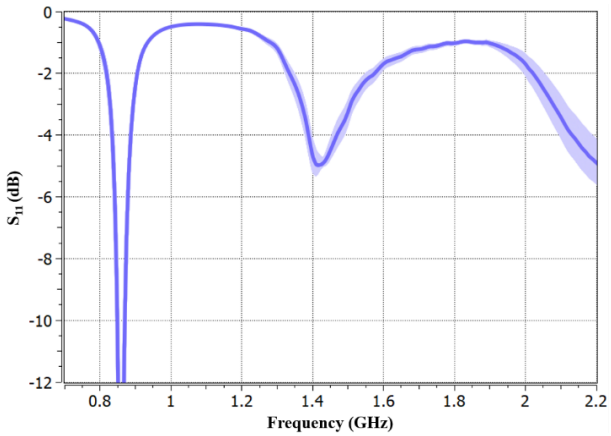


**FIGURE 16. Tolerance analysis of the SW3S ON state (840 – 880 MHz).**

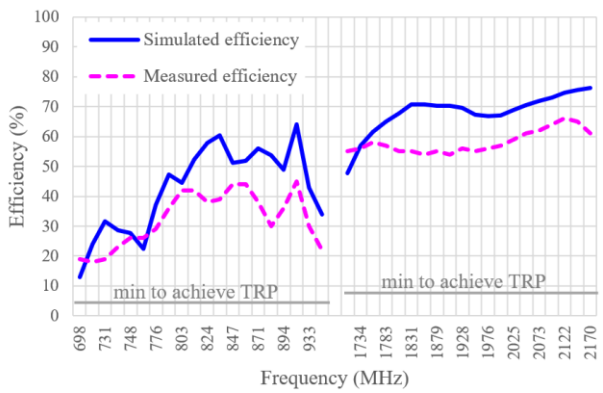


**FIGURE 17. Comparison between the simulated total efficiency and the measured total efficiency.**

The average total efficiency across all states in use (Figure 17) is 32.4% at 698 MHz – 960 MHz and 58.4% at 1710 MHz – 2170 MHz. The slight differences between the simulated and measured total efficiency are 1.1dB for the low-frequency region and 0.7dB for the high-frequency region, falling within the anechoic chamber specifications.

Total efficiency $\eta_t$ is measured in an anechoic chamber (MVG Star-Lab 18) (Figure 18). It includes losses of the PCB, the antenna element, the matching network, the SP4T and the UFL cable, this UFL has 0.1dB losses. The average difference between the simulated and the measured efficiency in the low-frequency band is 0.9dB, and in the high-frequency band is 0.4 dB.

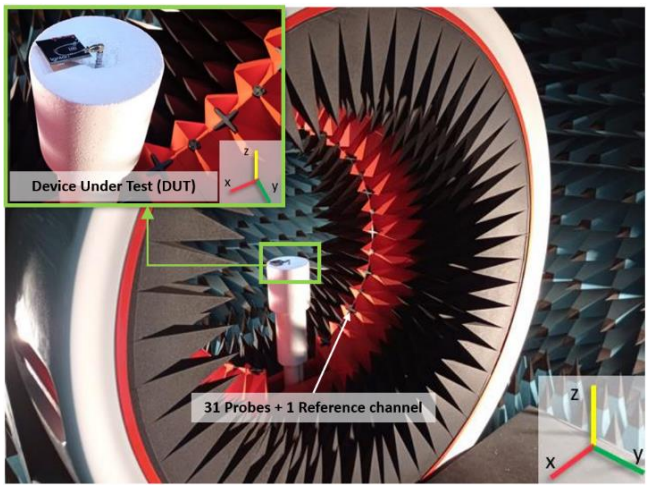


**FIGURE 18. Measurement set-up for total efficiency in the anechoic chamber**

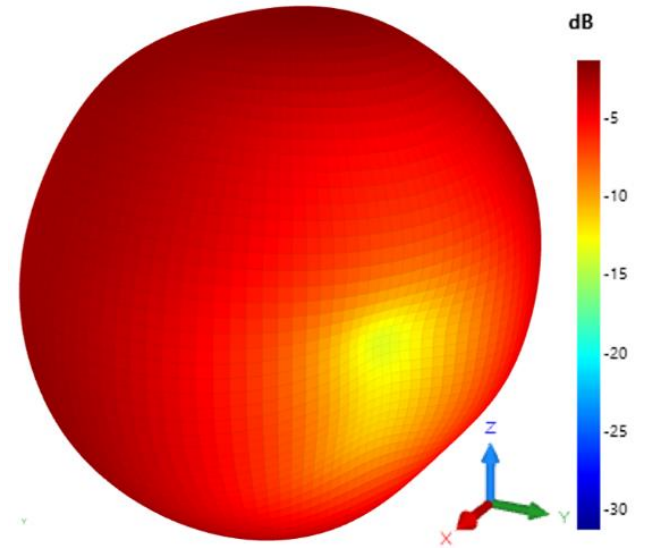


**FIGURE 19. Measured 3D radiation pattern showing the antenna realized gain at 800MHz.**

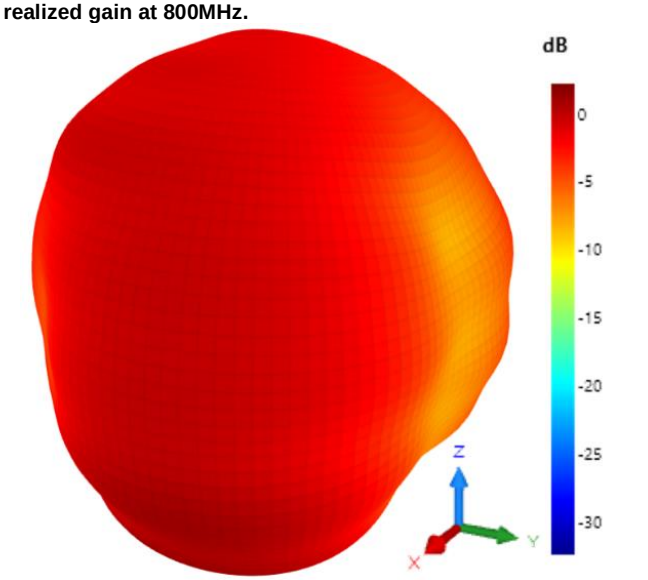


**FIGURE 20. Measured 3D radiation pattern showing the antenna realized gain at 2GHz.**

On the other hand, the radiation pattern of the antenna system is shown in (Figure 19) and (Figure 20), showing a quasi-isotropic pattern with directivity about 3dBi, useful in IoT devices since the direction of the incoming signal or the orientation of the device is random, which is a common situation in IoT communication.

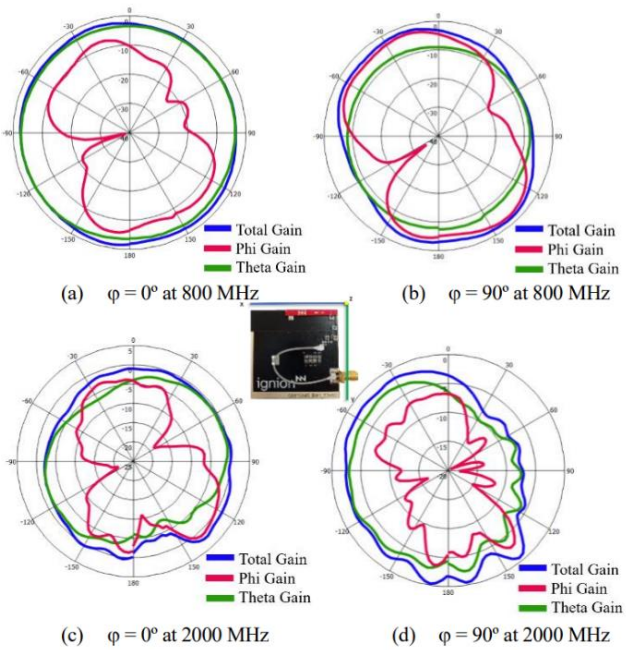


**FIGURE 21. Gain measured in MVG Star-Lab 18 of the PCB for two different frequencies. (a) φ = 0 at the frequency of 800 MHz; (b) φ = 90 at the frequency of 800 MHz; (c) φ = 0 at the frequency of 2000 MHz; (d) φ = 90 at the frequency of 2000 MHz.**

In (Figure 21), the isotropic behavior of the antenna system is shown. For example, at φ=0°, the radiation cuts are mainly omnidirectional with $G_\theta$ predominating over $G_\varphi$ and this, the polarisation is mainly linear aligned with the X-axis. However, polarization is less relevant than total efficiency for IoT devices since their orientation is random. Thus, it is not as critical as point-to-point antennas where polarisation alignment becomes relevant to avoid polarization mismatch. Additionally, the realized gain at various frequencies has been measured being -3.9 dB at 700 MHz, -1.4 dB at 800 MHz, -1.2 dB at 900 MHz, 1.8 dB at 1700 MHz, 2.5 dB at 1800 MHz, 1.9 dB at 1900 MHz, 2.2 dB at 2000 MHz and 2.4 dB at 2200 MHz; that is useful for link-budget calculations.

## V. DISCUSSION

This section highlights the advantages of employing the reconfigurable architecture over a passive solution featuring six components. The passive solution exhibits lower total efficiency, primarily because it struggles to achieve effective impedance matching across the entire frequency range, as demonstrated in (Figure 22).

Conversely, the current solution, utilizing one SP4T-Switch and five lumped components, outperforms for the whole frequency range, ensuring more range and battery life.

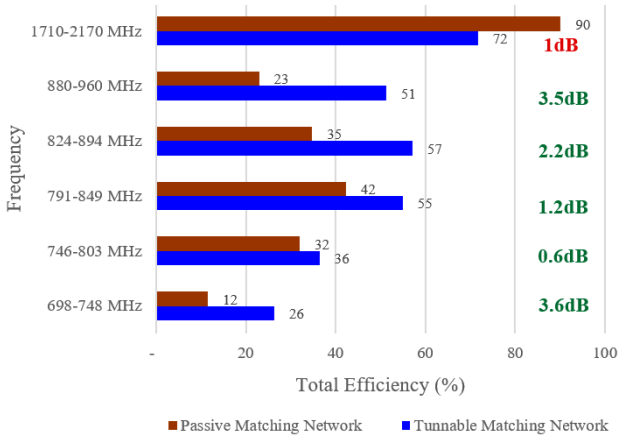


**FIGURE 22. Comparison between the simulated total efficiency with a passive network and the simulated total efficiency with the reconfigurable solution.**

In particular, a huge improvement of 3.8dB in 698 MHz – 748 MHz. At the high band, the reconfigurable solution is 1.2dB worst, but still, the efficiency for the tunable solution is 68% on average (Figure 22). In [22], a map of reconfigurable antennas, including both the length and width of the antenna dimensions, is conducted. The resulting average has a Length of 53,1mm and a Width of 9.8mm, and it leads to the conclusion that the antenna booster's reconfiguration-based solutions are in the best quadrant (L, W<average L, W).

Table V gathers different reconfigurable existing solutions compared to the proposed in this paper. As can be appreciated, the proposed solution features a small ground plane size, only compared to the small solution presented [22]. However, in the present case, efficiency in the low-frequency region (698 MHz – 960 MHz) is 3.7 dB above, plus the simplicity of using only one SP4T switch. In contrast, the compared devices [23], [24], [30] and [32] feature a larger ground plane in dimensions (0.35λ, 0.32λ, 0.47λ and 0.30λ) than the current solution (0.16λ), which implies a higher efficiency in the lower frequency bands. Moreover, [23] and [24] incorporate a metal frame, which is not viable for IoT devices due to cost. The innovative aspect of the proposed solution lies in its utilization of a single switch, with a more compact volume antenna booster, whereas [24] stands out for having the smallest clearance area despite incorporating a metal frame. As observed, the antenna volume is only 90mm$^3$, which is less than the metal frame structures in [23] and [24] and 26 times less than the antennas in [30] and [32].

Furthermore, thanks to this architecture, which includes 65 states, operational bandwidth can be extended to other frequency ranges, such as, for instance, those allocated in 600 to 700 MHz. For instance, for the proposed design, by having SW3S and SW1P ON, an $S_{11}$ below -6dB can be achieved.

TABLE V
COMPARISON WITH EXISTING RECONFIGURABLE ANTENNA SOLUTIONS. L IS THE MAXIMUM LENGTH OF THE PCB IN TERMS OF WAVELENGTH λ AT THE LOWEST FREQUENCY OF OPERATION. ANTENNA VOLUME IS THE SMALLEST PARALLELEPIPED INCLUDING THE ANTENNA

| | *PCB Size (mm$^2$)* | *$L_{PCB}$ (λ)* | *Antenna Volume (mm$^3$)* | *Clearance Area (mm$^2$)* | *Frequency (MHz)* | *Reconfigurability* | *Total Efficiency (low and high bands) (%)* |
|---|---|---|---|---|---|---|---|
| [22] | 131x60 | 0.30 | 12x3x2.4 = 86.4 | 11x60 = 660 | 698 – 960 and 1710 – 2690 | digitally tunable capacitors (DTC) and 7 lumped components | 53.5 and 62.8 |
| [22] | 50x50 | 0.11 | 30x3x1 = 90 | 12x40 = 480 | 698 – 960, 1575, and 1710 – 2170 | 2 SP8T switches and 11 lumped components | 13.6 and 47.4 |
| [23] | 130x67 | 0.35 | 945x5 = 4725 | 945 | 824–960 and 1710–2690 | PIN Diode | 45.0 and 60.0 |
| [24] | 143x74 | 0.32 | 146x5 = 730 | 146 | 690-960 and 1700 – 2700 | SP4T switch and 8 lumped components | 70.5 and 75 |
| [30] | 200x162 | 0.47 | 40x12x5 = 2400 | 12x200 = 2400 | 698 – 960 and 1710 – 2690 | SP4T switch and 4 lumped components | 63 and 64 |
| [32] | 130x70 | 0.30 | 40x10x6 = 2400 | 10x70= 700 | 698 – 960, 1710 – 2690 and 3500 – 3800 | digitally tunable capacitors (DTC) | 33, 63 and 63 |
| NEW | 70x65 | 0.16 | 30x3x1 = 90 | 15x45 = 675 | 698 – 960, and 1710 – 2170 | SP4T switch and 7 lumped components | 32.4 and 58.4 |

## VI. CONCLUSIONS

A reconfigurable architecture embedding an antenna booster element has been proposed. The architecture leverages a compact antenna booster element (λ/14 at 698MHz) in combination with an SP4T switch, including a straightforward matching network design. The key advantage of this architecture lies in the versatility it offers, as the SP4T switch enables the common port to be connected to various outputs, increasing flexibility in the impedance-matching process, this allows each band to be adapted separately, thereby achieving greater efficiency compared to the passive solution. After the proposed design process, the simulated total efficiency shows competitive efficiency values. The comparison between the simulated and measured efficiency results yielded minimal deviations, with a discrepancy of less than 0.9dB in the low-frequency band and 0.4dB in the high-frequency band. In practical testing, the implemented architecture achieved an average measured total efficiency of 32.4% at 698 MHz – 960 MHz and 58.4% at 1710 MHz – 2170 MHz. Notably, the proposed reconfigurable solution outperforms the passive alternative by up to 3.8dB in efficiency within the low-frequency range (698 MHz – 960 MHz). As a result, the proposed reconfigurable architecture with an embedded antenna booster element ensures operation across many frequency bands for IoT wireless devices.

## REFERENCES


[1] K. L. Wong, "Planar Antennas for Wireless Communications," Wiley, 2003.

[2] C. Rowell and E. Y. Lam "Mobile-Phone Antenna Design," *IEEE Antennas and Propagation Magazine*, vol. 54, no. 4, August 2012, pp.14-34.

[3] J. Anguera, A. Andújar, M. C. Huynh, C. Orlenius, C. Picher, and C. Puente, "Advances in Antenna Technology for Wireless Handheld Devices," *International Journal on Antennas and Propagation*, Volume 2013, Article ID 838364.

[4] The Institution of Engineering and Technology Seminar on Antennas and Propagation for Body-Centric Wireless Communications, "2007 IET Seminar on Antennas and Propagation for Body-Centric Wireless Communications", 2007.

[5] M. F. Iskander, Z. Yun, Z. Zhang, R. Isom, and M. Hawkins, "Antenna designs and propagation models for advanced wireless communications systems," *IEEE Antennas and Propagation Society International Symposium. Transmitting Waves of Progress to the Next Millennium*. 2000 Digest. (C, 2000, pp. 564-565 vol.2, doi: 10.1109/APS.2000.875208.

[6] M. Lai and S. Jeng, "Slot Antennas With an Extended Ground for Multiple-Antenna Systems in Compact Wireless Devices," *IEEE Antennas and Wireless Propagation Letters*, vol. 8, pp. 19-22, 2009, doi: 10.1109/LAWP.2008.920266.

[7] Z. X. Chen, Y. L. Ban, Z. Chen, K. Kang, and L. W. Li, "Two-strip narrow-frame monopole antenna with a capacitor loaded for hepta-band smartphone applications," *Prog. Electromagn. Res.*, vol. 145, no. 2, pp. 31–38, 2014.

[8] Y. L. Ban, C. L. Liu, J. L. W. Li, and R. Li, "Small-size wideband monopole with distributed inductive strip for seven-band WWAN/LTE mobile phone," *IEEE Antennas Wireless Propag. Lett.*, vol. 12, pp. 7–10, 2013.

[9] J. Anguera, A. Andújar, C. Puente, J. Mumbrú, "Antenna for Wireless Device Capable of Operation in Multiple Frequency Regions," *Patent Application WO* 2010/015364 A2, Feb.2010.

[10] A. Andújar, J. Anguera, and C. Puente, "Ground Plane Boosters as a Compact Antenna Technology for Wireless Handheld Devices," *IEEE Trans. Antennas Propag.*, 59, (5), p. 1668-1677, May 2011.

[11] J. Anguera, N. Toporcer, and A. Andújar, "Slim radiating systems for electronic devices," *US Patent* 9,960,478. May 2018.

[12] J. Anguera, C. Picher, A. Bujalance, and A. Andújar, "Ground Plane Booster Antenna Technology for Smartphones and Tablets," *Microwave and Optical Technology Letters*, vol.58, no. 6, pp.1289-1294, June 2016.

[13] J. Anguera, A. Andújar, C. Puente, and R. Mateos, "Modular multi-stage antenna system and component for wireless communications" *US Patent* 11,482,772 B2. Oct 2022.

[14] J. Rahola, "Optimization of matching circuits for antennas," *European Conference on Antennas and Propagation*, EuCAP 2011, Rome, Apr. 2011.

[15] J. Anguera, A. Andújar, C. Puente, "Multiband Antenna Booster Arquitecture with a single Switch", US. Pat. App. 63191334.

[16] A. Maunder, M. Rao, F. Robb, JM. Wild, "Comparison of MEMS switches and PIN diodes for switched dual tuned RF coils," *Magn Reson Med*. 2018; 80: 1746– 1753.

[17] Prem Pal Singh, Pankaj Kumar Goswami, Sudhir Kumar Sharma, and Garima Goswami, "Frequency Reconfigurable Multiband Antenna for IoT Applications in WLAN, Wi-MAX, and C-Band," *Progress In Electromagnetics Research C*, Vol. 102, 149-162, 2020.

[18] N. Hussain et al., "A Compact Flexible Frequency Reconfigurable Antenna for Heterogeneous Applications," *IEEE Access*, vol. 8, pp. 173298-173307, 2020, doi: 10.1109/ACCESS.2020.3024859.

[19] A. Vamseekrishna, B. T. P. Madhav, T. Anilkumar and L. S. S. Reddy, "An IoT Controlled Octahedron Frequency Reconfigurable Multiband Antenna for Microwave Sensing Applications," *IEEE Sensors Letters*, vol. 3, no. 10, pp. 1-4, Oct. 2019, Art no. 3502204, doi: 10.1109/LSENS.2019.2943772.

[20] Ullah, S. (2019). "A Tunable Microstrip Planar Antenna using Truncated Ground Plane for WiFi/LTE2500/WiMAX/5G/C, Ku, K-Band Wireless Applications". *International Journal of Electrical Engineering and Applied Sciences* (IJEEAS), 2(1), 77–84.

[21] S. Kingsly et al., "Multiband Reconfigurable Filtering Monopole Antenna for Cognitive Radio Applications," *IEEE Antennas and Wireless Propagation Letters*, vol. 17, no. 8, pp. 1416-1420, Aug. 2018, doi: 10.1109/LAWP.2018.2848702.

[22] J. Anguera, A. Andújar, J.L. Leiva, O. Massó, J. Tonnesen, E. Rindalsholt, R. Brandsegg, R. Gaddi, "Reconfigurable Multiband Operation for Wireless Devices Embedding Antenna Boosters," *Electronics* 2021, 10, 808.

[23] H.-B. Zhang, Y.-L. Ban, Y.-F. Qiang, J. Guo, and Z.-F.Yu, "Reconfigurable loop antenna with two parasitic grounded strips forWWAN/LTE unbroken-metal-rimmed smartphones," *IEEE Access*, vol. 5, pp. 4853-4858, 2017.

[24] L. Chen, Y. Huang, H. Wang, H. Zhou, and K. Liu, "A Reconfigurable Metal Rim Antenna With Smallest Clearance for Smartphone Applications," *IEEE Access*, vol. 10, pp. 112250-112260, 2022, doi: 10.1109/ACCESS.2022.3216237.

[25] F. Ferrero and L. H. Trinh, "868MHz Antenna Input Impedance Reconfiguration for IoT applications," *2022 IEEE Conference on Antenna Measurements and Applications (CAMA)*, Guangzhou, China, 2022, pp. 1-2, doi: 10.1109/CAMA56352.2022.10002585.

[26] T. Houret, L. Lizzi, F. Ferrero, C. Danchesi and S. Boudaud, "DTC-Enabled Frequency-Tunable Inverted-F Antenna for IoT Applications," in *IEEE Antennas and Wireless Propagation Letters*, vol. 19, no. 2, pp. 307-311, Feb. 2020, doi: 10.1109/LAWP.2019.2961114.

[27] Y. Chen, L. Zhang, Y. He, W. Li, and S. -W. Wong, "A Pattern Reconfigurable SIW Horn Antenna Realized by PIN Diode Switches," 2021 Computing, Communications and IoT Applications (ComComAp), 2021, pp. 112-115, doi: 10.1109/ComComAp53641.2021.9653080.

[28] A. M. Cayan and S. Basbug, "Four-Way Reconfigurable Repeater with U-Slot Microstrip Antennas for Outdoor IoT Applications," 2022 *11th International Conference on Renewable Energy Research and Application* (ICRERA), 2022, pp. 523-527, doi: 10.1109/ICRERA55966.2022.9922767.

[29] H. F. Abutarboush, R. Nilavalan, S. W. Cheung and K. M. Nasr, "Compact Printed Multiband Antenna With Independent Setting Suitable for Fixed and Reconfigurable Wireless Communication Systems," *IEEE Transactions on Antennas and Propagation*, vol. 60, no. 8, pp. 3867-3874, Aug. 2012, doi: 10.1109/TAP.2012.2201108.

[30] Y. L. Ban, S. C. Sun, P. -P. Li, J. L. -W. Li and K. Kang, "Compact Eight-Band Frequency Reconfigurable Antenna for LTE/WWAN Tablet Computer Applications," *IEEE Transactions on Antennas and Propagation*, vol. 62, no. 1, pp. 471-475, Jan. 2014, doi: 10.1109/TAP.2013.2287522.

[31] M. Borhani, P. Rezaei, and A. Valizade, "Design of a Reconfigurable Miniaturized Microstrip Antenna for Switchable Multiband Systems," *IEEE Antennas and Wireless Propagation Letters*, vol. 15, pp. 822-825, 2016, doi: 10.1109/LAWP.2015.2476363.

[32] L. H. Trinh, F. Ferrero, L. Lizzi, R. Staraj and J. -M. Ribero, "Reconfigurable Antenna for Future Spectrum Reallocations in 5G Communications," *IEEE Antennas and Wireless Propagation Letters*, vol. 15, pp. 1297-1300, 2016, doi: 10.1109/LAWP.2015.2505669.

[33] S. Caporal del Barrio, E. Foroozanfard, A. Morris and G. F. Pedersen, "Tunable Handset Antenna: Enhancing Efficiency on TV White Spaces," *IEEE Transactions on Antennas and Propagation*, vol. 65, no. 4, pp. 2106-2111, April 2017, doi: 10.1109/TAP.2017.2662221.

[34] J. Hannula, T. Saarinen, J. Holopainen, and V. Viikari, "Frequency Reconfigurable Multiband Handset Antenna Based on a Multichannel Transceiver," *IEEE Transactions on Antennas and Propagation*, vol. 65, no. 9, pp. 4452-4460, Sept. 2017, doi: 10.1109/TAP.2017.2725384.

[35] J. Deng, S. Hou, L. Zhao, and L. Guo, "Wideband-to-Narrowband Tunable Monopole Antenna With Integrated Bandpass Filters for UWB/WLAN Applications," *IEEE Antennas and Wireless Propagation Letters*, vol. 16, pp. 2734-2737, 2017, doi: 10.1109/LAWP.2017.2743258.

[36] Y. P. Selvam et al., "A Low-Profile Frequency- and Pattern-Reconfigurable Antenna," *IEEE Antennas and Wireless Propagation*

*Letters*, vol. 16, pp. 3047-3050, 2017, doi: 10.1109/LAWP.2017.2759960.

[37] P. -Y. Qin, F. Wei and Y. J. Guo, "A Wideband-to-Narrowband Tunable Antenna Using A Reconfigurable Filter," *IEEE Transactions on Antennas and Propagation*, vol. 63, no. 5, pp. 2282-2285, May 2015, doi: 10.1109/TAP.2015.2402295.

[38] S. Chilukuri, Y. P. Rangaiah, A. Lokam, and K. Dahal, "A Multi-Band Frequency and Pattern Reconfigurable Antenna for Wi-Fi/WiMAX and WLAN Applications: Frequency and Pattern Reconfigurable Antenna," *2018 9th International Conference on Mechanical and Aerospace Engineering* (ICMAE), 2018, pp. 208-212, doi: 10.1109/ICMAE.2018.8467558.

[39] T. N. Do, P. Thu Tran, and H. T. Le, "Study the Coexistence NB-IoT Paging and LTE Paging on eNodeB," *2020 IEEE Eighth International Conference on Communications and Electronics* (ICCE), 2021, pp. 80-84, doi: 10.1109/ICCE48956.2021.9352146.

[40] E. García, A. Andújar, J. L. Pijoan and J. Anguera, "Reconfigurable Antenna Booster Element for Multiband Operation in IoT Devices with an SP4T," *2023 17th European Conference on Antennas and Propagation (EuCAP)*, Florence, Italy, 2023, pp. 1-4, doi: 10.23919/EuCAP57121.2023.10133063.

[41] J. Anguera, A. Andujar, G. Mestre, J. Rahola and J. Juntunen, "Design of Multiband Antenna Systems for Wireless Devices Using Antenna Boosters [Application Notes]," in IEEE Microwave Magazine, vol. 20, no. 12, pp. 102-114, Dec. 2019, doi: 10.1109/MMM.2019.2941662.

[42] S. R. Best, "The inverse relationship between quality factor and bandwidth in multiple resonant antennas," *in Proc. IEEE Antennas and Propagation Society Int. Symp.*, 2006, pp. 623–626.

[43] AT&T Radiated Performance Requirements for IoT Devices, Public Release at www.att.com/iotdevices; TRP and TIS requirements for IoT devices [Online]. Available: radiated_performance_requirements_20200410103641282.pdf

**ELENA GARCÍA** telecommunication systems engineering and the M.S. degree in telecommunication engineering from La Salle, Ramon Llull University in 2020 and 2021, respectively. She is currently pursuing an industrial Ph.D. degree with La Salle, Ramon Llull University, and Ignion. Her current research interests include antenna booster design and antenna active solutions. She is currently working as an R&D researcher at Ignion.

**AURORA ANDÚJAR** was born in Barcelona, Spain, 1984. Founder partner at Ignion (VP of engineering, 2024 – up to date). She received the Bachelor and the Master degree in Telecommunications Engineering in 2005 and 2007, respectively. The Master degree of Science in Telecommunications Engineering and Management in 2007, and the Ph.D degree in 2013 from the Polytechnic University of Catalonia (UPC). In 2004-2005 she received a research fellowship in the field of Electromagnetic Compatibility by the UPC. In 2005 she worked as a Software Test Engineer in Tempos21. In 2006 she worked as a Software Engineer for Digital Campus in UPCnet. From 2007, she joined Fractus as R&D + I Engineer where she was in charge of the development of technological projects focused on the design of miniature and multiband antennas for wireless devices. She was also involved in the maintenance and growth of the patent portfolio of the company, including the development, writing, and prosecution of new inventions and patents (2007-2013). From 2013, she moves to the Product & Services Department, in 2015 she becomes Product Manager of the division, and in 2018 she was promoted to Senior Product and Business Development Manager. She was in charge of the development and release of new antenna products and led customer-oriented projects. In 2020, she became Director of Engineering, and she was in charge of leading the engineering department of the company, ensuring good engineering methodologies and practices for allowing the company to scale fast. In 2024 she became VP of Engineering leading the company's engineering strategy and development teams. Since 2009 she is leading research projects in the collaborative university-industry framework. From 2011 she became Assistant Professor at the Open University of Catalonia (UOC).

Dr. Andújar has more than 16 years of experience in the antenna industry. Author of more than 58 patents in the antenna field. She has published more than 125 papers in scientific journal, international, and national conferences. She has directed more than 80 bachelor and master thesis.

In 2015, Dr. Andújar received the award to the best doctoral thesis of Spain by the Spanish Association of Telecommunications Engineers (COIT-AEIT). As a research team in Fractus she received the Academiae Dilecta distinction by the Engineering Academy. Later, in 2016 she received the award to the best doctoral thesis in the scope of the TIC Engineering by the UPC. In 2021, she became finalist of the DonaTIC awards in the category of entrepreneur, organized by the department of the vice-presidency and digital and territorial policies of Catalonia, which have the dual aim of recognizing the fundamental role of women in the professional, business, and academic world while offering references to the sector. Early 2023, IGNION was the winner of the Innovative Company Award from the College of Graduate Engineers and Industrial Technical Engineers of Barcelona (ENGINYERS BCN), because its contributions to the redesign of the Internet of Things (IoT) connectivity, thanks to the creation of the next generation of multi-band, multi-purpose, and ready-to-use antenna chips.

**JOAN L. PIJOAN** is a Ph.D. in Electronics from Ramon Llull University - URL (2000), a Telecommunications Engineer from the Polytechnic University of Catalonia (1994), and a Telecommunications Technical Engineer from La Salle, Ramon Llull University (1991).

Since 1998, he has been a professor at the La Salle School of Electronic and Computer Engineering (Ramon Llull University) in the Department of Communications and Signal Theory. In 2004, he received the accreditation of lecturer, and in 2011, the accreditation of research, both issued by the Quality Agency of the Catalan University System (AQU). He has also been granted the six-year research periods 2004-2009, 2010-2015, and 2016-2021 period. In 2017 he obtained the category of Full Professor at Ramon Llull University. He is currently the coordinator of the Degree in Telecommunications Systems Engineering at the URL.

He was head of the Department of Communications and Signal Theory of the Ramon Llull University (2001-2011) and head of the Research Group on Electromagnetism and Communications (GRECO) (2000-2013) of the Ramon Llull University, a consolidated group recognized by the Generalitat de Catalunya in 2009. Due to a reorganization of the research groups, he belonged to the Research Group on Internet and Storage Technologies (GRITS) of the URL (2016-2022) and now belongs to the recently recognized Research Group on Smart Society. His research activity for the last 20 years has focused on channel sounding and modeling, the design of spread spectrum and multi-carrier modulations applied to broadband HF communications and Power Line communications, as well as the design of multi-user detectors in CDMA systems.

Since 2003, he has been investigating the use of broadband modulations in long-distance HF links between Antarctica and Spain, as well as the daily, seasonal, and annual variation of the parameters that characterize the ionosphere as a communication channel. Since 2013, he has experimented with using the Near Vertical Incidence Skywave (NVIS) technique for remote sensing and designing compact HF antennas.

Joan Lluís Pijoan is the author of more than 30 articles in magazines and more than 70 contributions at conferences. He has directed eight doctoral theses and more than 190 final degree projects. He has participated in 26 public and private research projects, being the principal investigator in 19 of them. It has also actively participated in the European stocks COST 262 Spread Spectrum Systems and Techniques in Wireless and Wired Communications and COST 289

Spectrum and Power Efficient Broadband Communications. He has participated as a reviewer for national and international scientific and technical publications and projects.

**JAUME ANGUERA** (S'99-M'03-SM'09-F'20) was born in Vinaròs, Spain, in 1972. Founder and CTO at Ignion; Associate Professor at Universitat Ramon Llull, both institutions in Barcelona, Spain.

He received a Technical Engineering degree in Electronic Systems and Engineering degree in Electronic Engineering, both from the Ramon Llull University (URL), Barcelona, Spain, in 1994 and 1998, respectively, and a Telecommunication Engineering degree (5 years degree) and a Ph.D. degree in Telecommunications, both from the Polytechnic University of Catalonia (UPC), Barcelona, Spain, in 1998 and 2003, respectively. From 1997 to 1999, he joined the Electromagnetic and Photonic Engineering Group of the Signal Theory and Communications Department of the UPC as a researcher in microstrip fractal-shaped antennas. In 1999, he was a researcher at Sistemas Radiantes, Madrid, Spain, where he was involved in designing dual-band dual-polarized fractal-inspired microstrip patch arrays for mobile communications. In the same year, 1999, he became Assistant Professor at the Department of Electronics and Telecommunications, Universitat Ramon Llull-Barcelona, and Associate Professor in 2016, where he teaches Antenna Theory and related courses and belongs to the recognised Research Group Smart Society. Since 2001, he has led research projects in the antenna field for wireless applications in a frame of Industry-University collaboration: Ignion and the Department of Electronics and Telecommunications of Universitat Ramon Llull-Barcelona, Spain. The Spanish Ministry and other institutions have awarded several of his supervised students Best Bachelor's and Master's Thesis.

From 1999-2017, he was with Fractus (founder partner) in Barcelona, Spain, where he held the position of R&D manager and developed various cutting-edge antenna technologies. At Fractus, he led projects for antenna products for base station antennas, automotive, and mobile phones.

Between 2003 and 2006, he was also assigned to Fractus in South Korea to head up the research team. One of his main tasks was to provide training, education, and development of the team's core competency and provide an R&D vision to address the rapidly growing mobile device market. Under his technical leadership, the company had secured major contracts with companies such as Samsung, LG, and Bellwave, to name a few. He published a book about "Korean Experiences" in 2015.

Since 2017, he has been with Ignion in the role of CTO. He leads the company's R&D activity to create new products and patents, envisages new technologies, and provides technology strategy and direction to scale the company's business.

He holds over 180 granted invention patents (USA, Asia, Europe) in the antenna field, many of which have been licensed and adopted by the wireless industry. Among his most outstanding contributions is that of the inventor of Antenna Booster Technology (commercially known as Virtual Antenna® technology), a technology that fostered the creation of Ignion. The wireless industry has adopted millions of these products globally to facilitate wireless connectivity for IoT (Internet of Things) devices, utilising a miniature component known as an antenna booster.

He is the author of more than 300 journal and international and national conference papers (h-index=55 with more than 9200 citations based on Google Scholar, in the top 1.4% of the ranking of Spanish researchers). He has given over 80 antenna lectures worldwide (USA, China, South Korea, India, UK, France, Germany, Poland, Czech Republic, Denmark, The Netherlands, Malta, Tunisia, Nigeria, Perú, Brazil, Canada, and Spain). He has directed over 170 bachelor's, master's, and Ph.D. theses. He has authored seven books.

Dr. Anguera has participated in over 24 national/international projects and research grants valued at over $14 million, many of which he was the principal researcher.

His research interests include antenna booster technology, multiband and small antennas, diversity antenna systems/MIMO, electromagnetic dosimetry, microstrip antennas, fractals, and genetically optimised antenna systems.

Dr. Anguera was a member of the fractal team that, in 1998, received the European Information Technology Grand Prize for Applied Science and Engineering for the fractal-shaped antenna application to cellular telephony. 2003 Finalist for the Best Doctoral Thesis on UMTS (Fractal and Broadband Techniques on Miniature, Multifrequency, and High-Directivity Microstrip Patch Antennas); prize promoted by "Technology plan of UMTS promotion" given by Telefónica Móviles España). New Faces of Engineering 2004 (promoted by IEEE and IEEE foundation). In the same year, he won the Best Doctoral Thesis (Ph.D.) in "Network and Broadband Services" (XXIV Prize Edition "Ingenieros de Telecomunicación") organised by Colegio Oficial de Ingenieros de Telecomunicación (COIT) and the Company ONO. In 2011, he received the Alè Vinarossenc recognition from Fundació Caixa Vinaròs. In 2014, together with four other Fractus inventors, he received the "2014 Finalist to European Patent Award". As a team in Fractus, we received the Technology Pioneer distinction from the World Economic Forum in 2005 and the Academiae Dilecta award from the Royal Academy of Engineering in 2015. As a team, Ignion has been awarded as the 2023 Innovative Company, awarded by Enginyers BCN in recognition of its disruptive Virtual Antenna® technology.

He is a reviewer for several IEEE journals. He is an associate editor at the IEEE Open Journal on Antennas and Propagation and Electronics Letters. His biography is listed in Who'sWho in the World, Who'sWho in Science and Engineering, Who'sWho in Emerging Leaders, and IBC (International Biographical Center, Cambridge-England). He is an IEEE Antennas and Propagation Distinguished Lecturer. He is the working group "Software and Modelling" vice-chair at EurAAP.

His detailed information can be found at: http://users.salleurl.edu/~jaume.anguera/